



Universiteit
Leiden
The Netherlands

Chitin in the fungal cell wall: Towards valorization of spent biomass of *Aspergillus niger*

Leeuwe, T.M. van

Citation

Leeuwe, T. M. van. (2020, November 4). *Chitin in the fungal cell wall: Towards valorization of spent biomass of *Aspergillus niger**. Retrieved from <https://hdl.handle.net/1887/138011>

Version: Publisher's Version

License: [Licence agreement concerning inclusion of doctoral thesis in the Institutional Repository of the University of Leiden](#)

Downloaded from: <https://hdl.handle.net/1887/138011>

Note: To cite this publication please use the final published version (if applicable).

Cover Page



Universiteit Leiden



The handle <http://hdl.handle.net/1887/138011> holds various files of this Leiden University dissertation.

Author: Leeuwe, T.M. van

Title: Chitin in the fungal cell wall: Towards valorization of spent biomass of *Aspergillus niger*

Issue date: 2020-11-04

CHAPTER 5

Rab GDP-dissociation inhibitor *gdiA* is an essential gene required for cell wall chitin deposition in *Aspergillus niger*

Tim M. van Leeuwe, Anne Gerritsen, Mark Arentshorst, Peter J. Punt, Arthur F.J. Ram

ABSTRACT

The cell wall is a distinctive feature of filamentous fungi, providing them with structural integrity and protection from both biotic and abiotic factors. Unlike plant cell walls, fungi rely on structurally strong hydrophobic chitin core for mechanical strength together with alpha- and beta-glucans, galactomannans and glycoproteins. Cell wall stress conditions are known to alter the cell wall through the signaling cascade of the cell wall integrity (CWI) pathway and can result in increased cell wall chitin deposition. A previously isolated set of *Aspergillus niger* cell wall mutants were screened for increased cell wall chitin deposition. UV-mutant RD15.8#16 was found to contain approximately 60% more cell wall chitin than the wild type. In addition to the chitin phenotype, RD15.8#16 exhibits a compact colony morphology and increased sensitivity towards SDS. RD15.8#16 was subjected to classical genetic approach for identification of the underlying causative mutation, using co-segregation analysis and SNP genotyping. Genome sequencing of RD15.8#16 revealed eight SNPs in open reading frames (ORF) which were individually checked for co-segregation with the associated phenotypes, and showed the potential relevance of two genes located on chromosome IV. *In situ* re-creation of these ORF-located SNPs in a wild type background, using CRISPR/Cas9 genome editing, showed the importance Rab GTPase dissociation inhibitor A (*gdiA*) for the phenotypes of RD15.8#16. An alteration in the 5' donor splice site of *gdiA* reduced pre-mRNA splicing efficiency, causing aberrant cell wall assembly and increased chitin levels, whereas gene disruption attempts showed that a full gene deletion of *gdiA* is lethal.

This chapter is published as: van Leeuwe, T.M., Gerritsen A., Arentshorst, M., Punt, P.J., Ram A.F.J., Fungal Genet. Biol. 136, 103319 (2020). doi: 10.1016/j.fgb.2019.103319

1. INTRODUCTION

The fungal cell wall is an essential structure that sets apart filamentous fungi from other eukaryotes. Mainly comprised of α -1,3-glucans, β -1,3-glucans, β -1,6-glucans and mixed β -1,3/1,4 varieties, chitin (β -1,4-linked-*N*-acetyl glucosamine), galactomannan and glycoproteins, the cell wall is continuously being built, remodeled, broken down and re-built to accommodate various stages and challenges of the filamentous lifestyle. For extensive review on cell wall organization and biosynthesis we refer to both Free, 2013 and Gow et al., 2017, with the references therein. In addition to the majority of glucans, chitin plays a structurally important part of the fungal cell wall for mechanical strength. At the plasma membrane, chitin synthases assemble the UDP-*N*-acetyl-glucosamine monomers into chitin polymers by extrusion of nascent chitin chains into the periplasmic space. Careful coordination of sufficient precursor and available chitin synthases at the plasma membrane, determine both the rate of which chitin is deposited into the cell wall and chitin chain length (Kang et al., 1984; Keller and Cabib, 1971; Orlean and Funai, 2019; Peter, 1987; Sburlati and Cabib, 1986). Seven clearly defined classes of chitin synthases (CHSI-CHSVII) are known to exist in filamentous fungi, some of which have been studied in detail, and have been shown to be correlated with morphogenesis and adaptation to ecological niches (Liu et al., 2017). Encompassing many different classes of chitin synthases, fungi temporally and spatially regulate expression during different stages of development. Additional post-translational activation of certain chitin synthases, involving glycosylation (Santos and Snyder, 1997; Trilla et al., 1999), phosphorylation (Valdivia and Schekman, 2003) and proteolytic cleavage of zymogenic chitin synthases (Choi et al., 1994) all contribute to tight regulation of chitin deposition in the cell wall.

As a result of this complex organization, levels of cell wall chitin are generally well maintained, and fluctuations in chitin content mainly differ depending differing stages of life cycle, environmental cues, mycelial age, available nutrients and cultivation conditions, hypoxia and stress (Lord and Vyas, 2019; Pochanavanich and Suntornsuk, 2002). Cell wall stress often results in increased cell wall chitin content through activation of the cell wall integrity (CWI) signal transduction pathway (Fortwendel et al., 2010; Heilmann et al., 2013; Ram et al., 2004; Walker et al., 2015, 2008). This conserved, natural response in filamentous fungi often involves a compensatory increase in both cell wall chitin and alpha-glucan deposition. Specifically, under cell wall stress conditions in *A. niger* it was reported that levels of both *agsA* (alpha-glucan synthase A) (Damveld et al., 2005b) and *gfaA* (glutamine-fructose-6-phosphate-amidotransferase A) (Ram et al., 2004) are induced. The expression of the former was previously used in a cell wall stress reporter system to identify mutants with a constitutively activated cell wall stress response in a UV-screen (Damveld et al., 2008). We identified mutants from this cell wall mutant library that display an increased cell wall chitin content (**Chapter 4**). Resultant from this screen, mutant RD15.8#16 was identified as a strain with increased cell wall chitin levels.

In the quest to identify the genotype related to the cell wall phenotype of RD15.8#16, we took a classical genetics approach combined with genome sequencing. A lacking established sexual cycle of *A. niger* prevents traditional type crossings, however, a parasexual cross was used instead

to obtain segregants (Arentshorst and Ram, 2018; Pontecorvo et al., 1953; Swart et al., 2001). It is important to note in this approach that, unlike a conventional sexual cycle, cross-over events are singularly mitotic and are therefore relatively rare. When cross-over events are absent, co-segregation analysis is only indicative of the linked chromosome, rather than a specific gene or genomic region.

In this study, we performed co-segregation analysis of the RD15.8#16 phenotype by selecting segregants that displayed either wild type or the RD15.8#16 phenotypes. Segregants with either of the two phenotypes were checked for presence of SNPs that are unique to RD15.8#16. Comparative SNP analysis revealed the chromosomal distribution among segregants and identified the exclusive co-segregation of markers on chromosome IV with the RD15.8#16 phenotype. With the use of a previously reported CRISPR/Cas9 gene editing system (**Chapter 2**), we performed *in situ* SNP editing of the endogenous wild type allele to re-create the respective mutant alleles on chromosome IV. Re-creation of mutant alleles in a wild type genetic background revealed that inefficient and/or aberrant splicing of Rab GDP-dissociation inhibitor (*gdiA*) is responsible for the phenotype of RD15.8#16.

2. MATERIALS AND METHODS

2.1 Strains, media, growth conditions

Strains used in this study can be found in Table 1. All media were prepared as described by Arentshorst et al., 2012. In all cases, minimal medium (MM) contained 1% (w/v) glucose, 1.5% agar and was supplemented when required with 10mM uridine and 2.5 µg/mL nicotinamide. To test the presence or absence of the *amdS* gene, MM acetamide agar (MM-AA) was used as described by Arentshorst et al., 2012. Complete medium (CM) contained 1% (w/v) glucose, 1.5% agar (Scharlau, Barcelona, Spain), 0.1% (w/v) casamino acids and 0.5% (w/v) yeast extract in addition to MM. Strains were inoculated from -80°C glycerol stocks onto fresh CM plates and were allowed to grow and sporulate for 5-7 days at 30°C, prior to spore harvesting. Spores were harvested by addition of 15 mL of 0.9% (w/v) NaCl to CM spore plates and were carefully scraped from the surface with a cotton swab. Spore solutions were poured over sterile cotton filters (Amplitude™ Ecocloth™ Wipes, Contec Inc., Spartanburg, SC, USA) to remove large mycelial debris. Spore solutions were counted using Bio-Rad TC20™ Automated Cell Counter (Bio-Rad Laboratories, Inc. USA) using Counting Slides, Dual Chamber for Cell Counter (Cat#145-0011, Bio-Rad Laboratories, Inc. USA).

2.2 SDS sensitivity assays

Wild type, mutants and segregants were tested on different concentrations of SDS. Using a 10% (w/v) SDS stock, MM plates (when required, supplemented with either or both uridine and nicotinamide) to create final SDS concentrations of 0.004%, 0.0045% and 0.005% SDS. Spore stocks were created as described above. Spores were counted, serially diluted into 2000, 200, 20

and 2 spores/ μL and 5 μL of respective dilutions were spotted on MM SDS plates. The plates were incubated for 96h at 30 °C prior to scoring phenotypes.

SDS sensitivity was tested with un-normalized spore concentrations during the segregants screen. A total of 200 segregants and controls were streaked twice on MM + U + N and spores were harvested from a single colony using a pre-wetted (0.9% NaCl) cotton swab. Cotton swab containing spores was dipped and swirled in 0.5 mL 0.9% NaCl to dissolve spores. For each segregant and control strain, 5 μL spore solution was spotted on plates for testing phenotypes (see section 2.4).

Table 1. All strains used in this study

Name	Genotype	Reference
N402	<i>cspA1</i>	Bos et al., 1988
MA234.1	<i>cspA1, ΔkusA::DR-<i>amdS</i>-DR</i>	Park et al., 2016
MA169.4	<i>cspA1, ΔkusA::DR-<i>amdS</i>-DR, <i>pyrG</i></i>	Carvalho et al., 2010
RD15.8	<i>cspA1, <i>pyrG</i>, <i>PagsA-H2B-GFP-TrpC-pyrG*</i>, <i>PagsA-<i>amdS</i>-TamdS</i> + <i>pAN7-1 (hph+)</i></i>	Damveld et al., 2008
RD15.8#16	UV-mutant of RD15.8	Damveld et al., 2008
TLF56	RD15.8#16, <i>pyrG</i> (5'-FOA selected)	This study
TLF54	RD15.8#16, <i>pyrG</i> (5'-FOA selected), Δ <i>brnA</i>	This study
JN6.2	<i>cspA1, ΔkusA::DR-<i>amdS</i>-DR, <i>pyrG</i>-, <i>nicB::hygB</i>, <i>olvA::AOpyrG</i></i>	Niu et al., 2016
TLF92	Diploid strain: JN6.2 x TLF54	This study
AG1	NRRL3_05482 mutant allele in MA234.1	This study
AG3	<i>gdiA</i> mutant allele in MA234.1	This study
Δ <i>olvA</i> #8	Segregant of TLF92, Δ <i>olvA::AOpyrG</i> , <i>nicB</i> *, <i>amdS</i> *	This study
Δ <i>olvA</i> #27	Segregant of TLF92, Δ <i>olvA::AOpyrG</i> , <i>nicB</i> *, <i>amdS</i> *	This study
Δ <i>olvA</i> #41	Segregant of TLF92, Δ <i>olvA::AOpyrG</i> , <i>nicB</i> *, <i>amdS</i> *	This study
Δ <i>olvA</i> #50	Segregant of TLF92, Δ <i>olvA::AOpyrG</i> , <i>nicB</i> *, <i>amdS</i> *	This study
Δ <i>olvA</i> #67	Segregant of TLF92, Δ <i>olvA::AOpyrG</i> , <i>nicB</i> *, <i>amdS</i> *	This study
Δ <i>brnA</i> #4	Segregant of TLF92, Δ <i>brnA</i> , <i>pyrG</i> *, <i>nicB</i> *, <i>amdS</i> *	This study
Δ <i>brnA</i> #11	Segregant of TLF92, Δ <i>brnA</i> , <i>pyrG</i> *, <i>nicB</i> *, <i>amdS</i> *	This study
Δ <i>brnA</i> #25	Segregant of TLF92, Δ <i>brnA</i> , <i>pyrG</i> *, <i>nicB</i> *, <i>amdS</i> *	This study
Δ <i>brnA</i> #33	Segregant of TLF92, Δ <i>brnA</i> , <i>pyrG</i> *, <i>nicB</i> *, <i>amdS</i> *	This study
Δ <i>brnA</i> #53	Segregant of TLF92, Δ <i>brnA</i> , <i>pyrG</i> *, <i>nicB</i> *, <i>amdS</i> *	This study
Δ <i>brnA</i> #77	Segregant of TLF92, Δ <i>brnA</i> , <i>pyrG</i> *, <i>nicB</i> *, <i>amdS</i> *	This study
Δ <i>brnA</i> #90	Segregant of TLF92, Δ <i>brnA</i> , <i>pyrG</i> *, <i>nicB</i> *, <i>amdS</i> *	This study

2.3 Cell wall isolation and chitin analysis

2.3.1 Cell wall isolation

Strains were cultured to obtain equally aged spores as described above. To 25mL of liquid CM (100mL Erlenmeyer flask), a final concentration of 10^6 spores/mL was added and grown overnight for 17h at 30°C, 200 rpm. Mycelium was harvested by applying a vacuum over a Whatman™ Glass Microfiber Filter (GF/C™) (diameter 47 mm, CAT No.1822-047, Buckinghamshire, UK) to remove medium and capture and dry the mycelium. Dried mycelium was frozen in liquid N₂ prior to grinding in order to break open the cells with mortar and pestle into a fine powder. Next, samples were washed to remove intracellular debris and proteins: washing occurred by addition of 50 mL 1M NaCl, followed by three washing steps with 50mL MQ. In both cases washing involves vigorous shaking and vortexing with 25 mL volume in 50 mL plastic tubes (114x28mm, Sarstedt AG & Co. KG, 62.547.254). Subsequently, the remaining 25 mL volume was added followed by repeated shaking and vortexing. Cell wall suspensions were centrifuged at 3,500 rpm for 10 min. to pellet cell walls. Supernatant was carefully discarded prior to the next washing step. Cell walls were lyophilized after washing steps for 48h.

2.3.2 Cell wall hydrolysis and chitin analysis

Chitin was measured as total glucosamine and was performed based on the principle of the Morgan-Elson protocol (Elson and Morgan, 1934) and was adapted for higher through-put analysis, using a 96-well plate reader. See appendix (Supplementary document 1) for a detailed description of the protocol. Due to variability between separate experiments in absolute glucosamine content, a wild type control was always included every time to compare relative differences. Cell wall glucosamine measurements from independent replicate experiments are expressed as means ± SEM. The statistical analysis was carried out using software R studio (Version 1.1.456) (RStudio: Integrated Development for R. RStudio, Inc., Boston, 2016). For total cell wall glucosamine experiments, we used one-way ANOVA. Significant differences between groups were subjected to posthoc Tukey multiple-comparisons analysis. Significance levels are indicated as $p < 0.05$ (*), $p < 0.005$ (**), $p < 0.001$ (***) and $p < 0.0001$ (****).

2.4 Parasexual cycle and segregant analysis

Formation of heterokaryons and selection for diploids was performed as described previously described (Arentshorst and Ram, 2018). Requirements for this procedure are for each strain to have separate auxotrophic deficiencies and different color markers from one of the three known complementation groups involved in melanin production: fawn (*fwnA*, NRRL3_00462, An09g05730), olive (*olvA*, NRRL3_01039, An14g05350) or brown (*brnA*, NRRL3_01040, An14g05370) colored (Jørgensen et al., 2011). As such, two haploid strains are coerced to fuse without supplementation for their respective auxotrophic deficiencies. This process yields a heterokaryotic, prototrophic mycelium in which karyogamy can occur at a very low frequency, resulting in a diploid strain. Due to the primarily uninuclear nature of *A. niger* asexual spores, color

markers help identify whether nuclei have fused, and become black as a result of complementing alleles from the other chromosome, or remain unfused as one of the individual colors in the heterokaryotic mycelium. An obtained diploid contains both chromosome-sets and can be haploidized to allow random distribution of each chromosome by exposure to benomyl, creating auxotrophic, brown- or olive-colored segregants. To obtain an auxotrophic haploid derivative of RD15.8#16, this strain was subjected to 5'-FOA counter selection to lose the *pyrG* (Arentshorst et al., 2015; Boeke et al., 1984), resulting in strain TLF56 (Table 1). TLF56 was subsequently transformed with pFC330_ *brnA*-sgRNA (pTLL37.1) and a knockout repair DNA fragment as described previously (**Chapter 2**).

Segregation of diploids was performed at 0.4 µg/mL benomyl on complete medium (CM) supplemented with 10mM uridine and 2.5 µg/mL nicotinamide. Segregants were single streaked twice on MM with uridine and nicotinamide prior to segregation analysis. Auxotrophic marker distribution and SDS sensitivity were tested for all 200 segregants. Spores were taken from a single colony of the second single streak with a pre-soaked cotton swab (using 0.9% w/v NaCl solution) and taken up into 500 µL 0.9% (w/v) NaCl. For each segregant, 5 µL spore solution was spotted on MM + uridine + nicotinamide, MM + uridine and MM-AA + uridine + nicotinamide and on MM + uridine + nicotinamide + 0.005% SDS. These were incubated for 144h at 30 °C.

2.5 DNA isolation, Illumina sequencing and SNP analysis

Genomic DNA was isolated as described by Arentshorst et al., 2012. In case of genome sequencing, this procedure was followed by column purification using the Nucleospin Plant II kit (Machery-Nagel), according to the manufacturer's instructions. Genome sequencing was executed by GenomeScan B.V (Leiden, The Netherlands). The NEBNext® Ultra DNA Library Prep kit for Illumina (cat# NEB #E7370S/L) was used to process the samples. Fragmentation of the DNA using the Biorupor Pico (Diagenode), ligation of sequencing adapters, and PCR amplification of the resulting product was performed according to the procedure described in the NEBNext Ultra DNA Library Prep kit for Illumina Instruction Manual. The quality and yield after sample preparation was measured with the Fragment Analyzer. The size of the resulting product was consistent with the expected size of approximately 500-700 bp. Clustering and DNA sequencing using the Illumina cBot and HiSeq 4000 was performed according to manufacturer's protocols. A concentration of 3.0 nM of DNA was used. HiSeq control software HCS v3.4.0 was used. Image analysis, base calling, and quality check was performed with the Illumina data analysis pipeline RTA v2.7.7 and Bcl2fastq v2.20. SNP calling was performed according to GenomeScan Guidelines Small Variant Analysis v3.0. The Variant Call Format (VCF) files were manually analyzed by the authors. Frequency score of identical SNP call boundary was set to ≥ 0.75 , while sequencing depth was left unselected.

2.6 Co-segregation analysis of SNPs

Approximately 400-500 bp long PCR products surrounding the SNP in question were amplified with primers listed in Primer Table. An additional nested primer was designed for each PCR

product used for sequencing. Sequencing of individual SNPs was performed using Sanger sequencing (Macrogen Europe, Amsterdam, The Netherlands). Analysis of sequencing data and alignments were performed in Benchling [Biological Software] 2019.

2.7 Single gene knockouts using split marker fragments

MA169.4 (Table 1) was transformed after protoplastation as described previously (Arentshorst et al., 2012). Using the split marker approach for single gene knockouts, entire ORFs were deleted by replacement with the *Aspergillus oryzae pyrG* (*AOpyrG*) selection marker (Arentshorst et al., 2015). Flanks were generated via PCR using N402 genomic DNA as template and primers as described in Primer Table. *AOpyrG* fragments were obtained from plasmid pAO4-13 (de Ruiter-Jacobs et al., 1989) with primers as described in Primer Table. Fusion PCR was used to generate split marker fragments containing *AOpyrG*. Approximately 2 µg of DNA per flank was added to protoplasts for transformation. Transformation plates were incubated on MMS for 6 days at 30°C. Transformed colonies were single streaked on MM twice for purification and were genotyped using diagnostic PCR (data not shown).

2.8 SNP re-creation in a wild type background using CRISPR/Cas9 gene editing

SNPs were introduced in a wild type (MA234.1) background using CRISPR/Cas9 mediated gene editing with a marker-free repair DNA fragment (**Chapter 2**). All primers are listed in Primer Table. Primers OTL479 and OTL480 were used in combination with pTE1_rev and pTE1_for, respectively, to obtain a sgRNA construct to target the wild allele NRRL3_05482 in MA234.1. Similarly, for NRRL3_06010, primers OTL477 and OTL476 were used in combination with pTE1_rev and pTE1_for, respectively, to obtain a sgRNA construct to target the wild allele NRRL3_06010 in MA234.1. Plasmids pTLL108.1 and pTLL109.2 were used as template DNA for sgRNA flanks. Flanks were fused through PCR to obtain sgRNAs, and cloning of the sgRNAs into pFC332 resulted in pFC332_NRRL3_05482-sgRNA and pFC332-NRRL3_06010-sgRNA. Marker-free repair DNA fragment for NRRL3_05482 was obtained through fusion PCR, 5' flank was amplified using OTL481 and OTL482, whereas 3' flank was amplified with OTL483 and OTL484. OTL482 and OTL483 contained a single mismatch to introduce a point mutation (see section 3.5) and allowed sufficient overhang for generation of a fusion construct. Marker-free DNA fragment repair for NRRL3_06010 was amplified from RD15.8 as template DNA, using OTL485 and OTL486. CRISPR/Cas9 plasmid transformations were performed after protoplastation as described previously (**Chapter 2**), using a pFC332 (*hph*) plasmid (Nødvig et al., 2015): 2 µg of Cas9-sgRNA plasmid with approximately 2 µg of repair DNA fragment for transformation. Transformation plates were incubated on MMS with 200 µg/mL hygromycin for 7 days at 30°C. Transformed colonies were single streaked on selectable MM with 100 µg/mL hygromycin to select for the presence of the Cas9-sgRNA plasmid. Next, a single colony was picked and transferred to non-selective MM medium to allow loss of the Cas9-sgRNA plasmid. A third streak of a single colony on both MM and MM with 100 µg/mL hygromycin uridine was performed as a control for loss of plasmid. DNA from plasmid-cured strains was isolated as described by Arentshorst et al., 2012, using mortar

and pestle to grind the mycelium in liquid nitrogen. Genotypes were confirmed using diagnostic PCR. Diagnostic PCR fragments from wild type (RD15.8), mutant (RD15.8#16) and transformants were sent for sequencing to check for SNP alterations (Macrogen Europe, Amsterdam, The Netherlands).

2.9 RNA isolation and RT-PCR for cDNA

RNA was isolated and column purified according to Park et al., 2016. Complementary DNA (cDNA) was obtained using the QuantiTect Reverse Transcription Kit (Qiagen). In short, 1 µg of RNA was added to 2 µL of gDNA Wipeout Buffer and RNase-free water was added to a total volume of 14 µL. After incubation for 2 min at 42 °C, the reactions were placed on ice. Then Reverse-transcription master mix (1 µL), Quantiscript RT Buffer (4 µL) and RT Primer Mix (1 µL) were added and the RT-reaction was performed for 15 min at 42 °C, followed by a heat inactivation step of 3 min at 95 °C. 1 µL of the resulting cDNA library was used as template in subsequent PCR experiments.

3. RESULTS

3.1 RD15.8#16 displays a compact colony morphology, SDS sensitivity and increased cell wall chitin

RD15.8#16 was selected from a previously obtained set of cell wall stress mutants (Damveld et al., 2008), and was found in a screen for strains with an increased cell wall chitin content (**Chapter 4**). Increased cell wall chitin was suggested by increased Calcofluor White (CFW) staining (Figure 1A). Next, total glucosamine content from cell wall dry weight was measured for the wild type strain N402 (159 µg/mg ± 5.01, n=3), parental strain RD15.8 (163 µg/mg ± 8.73, n=3) and UV-mutant RD15.8#16 (263 µg/mg ± 7.80, n=3) and is depicted in Figure 1B. Whereas the wild type and parental reporter strain have equal amount of cell wall glucosamine, RD15.8#16 shows a respective increase of 61% chitin. In addition to the cell wall phenotype, the mutant has a compact colony morphology and has increased sensitivity towards SDS (Figure 1C).

3.2 A parasexual cross and segregation analysis to isolate linkage to SDS sensitivity

To perform a parasexual cross and subsequent detection of segregation of diploid strains, we used a derivative strain of RD15.8#16 harboring *ΔbrnA*, *pyrG*⁻, strain TLF54 (see section 2.4). A previously obtained olive-colored, *nicB* wild type strain JN6.2 (*ΔnicB::AOpyrG*, *ΔolvA::hygB*, (Niu et al., 2016b), Table 1) was used to perform a parasexual cross with TLF54.

Figure 1C shows an SDS sensitivity phenotype for RD15.8#16 used for segregants screening. Prior to segregant analysis, both parental strains JN6.2 and TLF54 were checked against their non-auxotrophic, non-color deficient counterparts RD15.8 and RD15.8#16, respectively. As is evident from Figure 2, both parental strains for the parasexual cross show the same level of SDS sensitivity as their parental counterparts. Additionally, colony morphologies of RD15.8#16 and TLF54 are identical and show a more compact growth style than both JN6.2 and RD15.8.

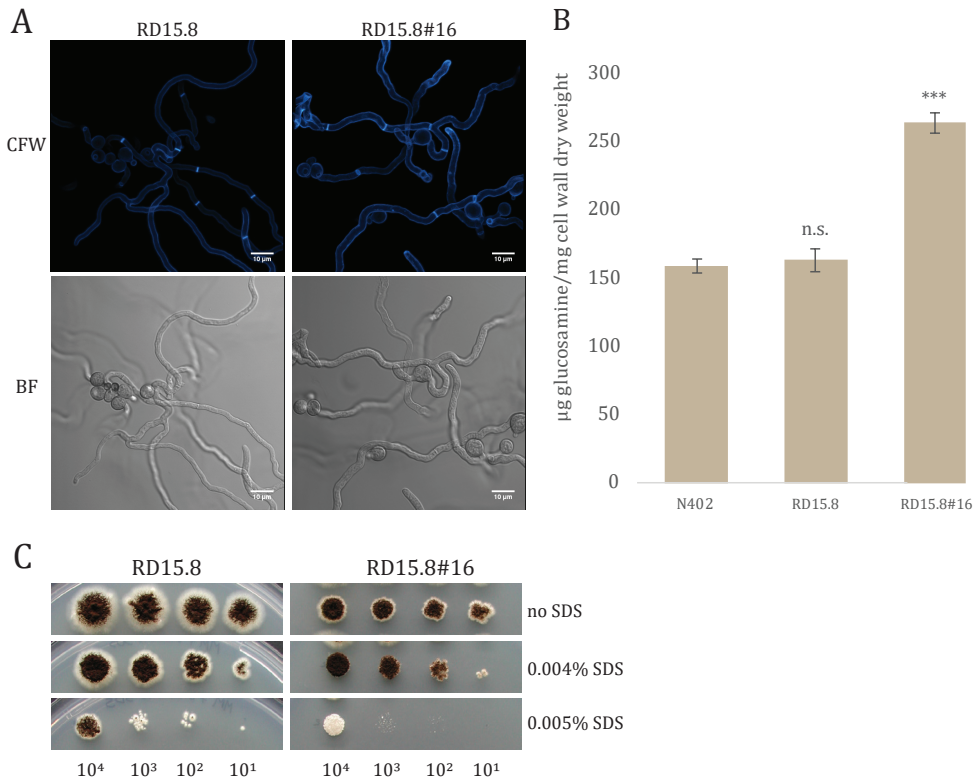


Figure 1. Chitin content and morphology of UV-mutant and wild types. (A) Chitin content of N402, RD15.8 (parent) and RD15.8#16 are shown (n=3). (B) Growth morphology on MM, and SDS sensitivity on MM + SDS for RD15.8 and RD15.8#16. Statistical methods and significance is described in section 2.3.2. Listed significant differences are compared to N402. Abbreviation n.s. refers to not significant. (C) SDS sensitivity of RD15.8 and RD15.8#16 on minimal medium (described in section 2.1) with either no SDS, 0.004% SDS or 0.005% SDS. (section 2.2). Spore amounts (#) per spot from left to right are 10^4 , 10^3 , 10^2 or 10^1 , and are listed below the figure. Strains were incubated 96h at 30°C.

Morphologies of wild type JN6.2, TLF54, original mutant RD15.8#16 and diploid TLF92 are shown on CM and CM + 0.5 μg/mL benomyl in Supplementary figure 1. The diploid strain TLF92 forms black spores, indicating that all spores contain two sets of chromosomes by color complementation of *brnA* and *olvA*. On CM + 0.5 μg/mL benomyl, the diploid strain forms sectors of both brown and olive colors that represent chromosomal loss from diploid to haploid (Supplementary figure 1).

In total 200 segregants were screened for SDS sensitivity by spotting spores on MM + U + N + 0.005% SDS, and for colony morphology resembling TLF54. Only two out of 200 segregants were found to display the same compact phenotype of TLF54 and were prone to SDS sensitivity (Supplementary figure 2A and B, segregants $\Delta brnA\#53$ and $\Delta brnA\#90$). Two randomly picked segregants, $\Delta olvA\#27$ and $\Delta olvA\#41$ resembling both wild type-like morphology and wild type-like SDS sensitivity, were taken in addition to $\Delta brnA\#53$ and $\Delta brnA\#90$ for a closer comparative analysis SDS sensitivity with normalized spore concentrations (Figure 3A). Evidently, we confirmed that $\Delta brnA\#53$ and $\Delta brnA\#90$ are indeed equally sensitive to SDS as TLF54. The chitin content of the cell wall was analyzed by determining the total cell wall glucosamine content of

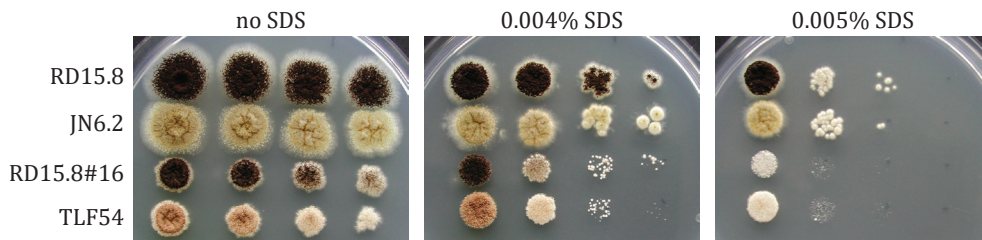


Figure 2. Morphology of strains involved in parasexual cross. SDS sensitivity spot assay of RD15.8, JN6.2, RD15.8#16 and TLF54 on 0.004% and 0.005% SDS in Minimal Medium (MM) with 10mM uridine (U) and 2.5 µg/mL Nicotinamide (N). From left to right, spore count equals 10^4 , 10^3 , 10^2 and 10^1 . Strains were incubated 96h at 30°C.

$\Delta brnA\#53$ and $\Delta brnA\#90$, parental strains JN6.2, TLF54 and segregants $\Delta olvA\#27$, $\Delta olvA\#41$. Figure 3B shows a comparative analysis of glucosamine content of the aforementioned strains versus the wild type parent JN6.2. Both $\Delta brnA\#53$ and $\Delta brnA\#90$ showed a significant increase in cell wall glucosamine versus JN6.2, but were not significantly different from TLF54. In addition, segregants $\Delta olvA\#27$ and $\Delta olvA\#41$ do not differ significantly from JN6.2. These data suggest that both $\Delta brnA\#53$ and $\Delta brnA\#90$ inherited all the associated phenotypes of TLF54 and that the SDS sensitivity and increased cell wall chitin are caused by the same mutation.

Due to very unequal segregation of mutant traits, we checked for chromosome distribution among segregants based on the other available genetic markers. As *brnA* and *olvA* are located adjacent to each other on chromosome I, we initially picked a total of 100 brown and 100 olive segregants segregating TLF92 diploid strain to obtain equal numbers of segregants in which one of the copies of chromosome I was present. Equal distribution of wild type and mutant of chromosomes was also checked for chromosome III and VII using the markers located on either chromosome

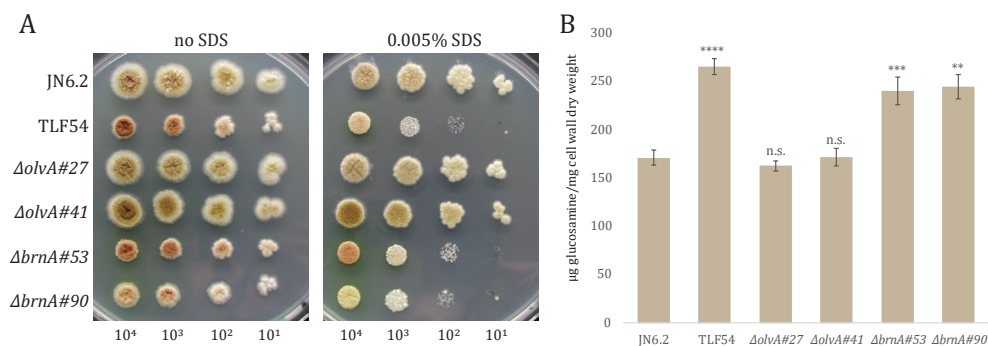


Figure 3. Phenotypes of parental strains JN6.2, TLF54, and segregants thereof. (A) Parents from parasexual cross JN6.2 and TLF54, two non-SDS sensitive segregants ($\Delta olvA\#27$ and $\Delta olvA\#41$) and two SDS sensitive strains ($\Delta brnA\#53$ and $\Delta brnA\#90$). Colony morphology and SDS sensitivity (0.005%) in Minimal Medium (MM) with 10mM uridine (U) and 2.5 µg/mL nicotinamide (N) grown at 30°C for 96h. (B) Cell wall glucosamine of all strains grown in Complete medium (CM) with U and N at 30°C for 17h (n=3-6)*. Statistical methods and significance are described in section 2.3.2. Listed significant differences are compared to JN6.2. Abbreviation n.s. refers to not significant. *variable sample size.

Table 2. Genomic single nucleotide polymorphisms (SNPs) of TLF54. SNPs located inside open reading frames (ORFs) of TLF54.

Chr	NRRL3_ID	CBS513.88 ID	Gene description	ORF strand	WT	TLF54	Effect of SNP on codon sequence
I	NRRL3_01084	An14g05970	Multi antimicrobial extrusion family protein	-	C	G	Codon change: Gln ^{382/504} --> Gln ^{382/504}
II	NRRL3_01535	An13g00450	Hypothetical protein	-	C	T	Codon change: Leu ^{305/347} --> Val ^{305/347}
II	NRRL3_01607	An01g00340	Solute carrier family 35 member	+	C	CCTT	13 th base of 1 st intron (CT rich region)
III	NRRL3_03466	An12g03570	<i>pyrG</i>	+	G	GGATC	Frameshift: Pro ^{255/277} --> Arg ^{255/277}
IV	NRRL3_05482	An02g09460	C2H2-type and FYVE-type zinc finger containing protein (Yeast ortholog PEP7; adaptor protein involved in vesicle-mediated vacuolar protein sorting)	+	C	T	Codon change: His ^{299/675} --> Tyr ^{299/675} (between two FYVE-type zinc fingers)
IV	NRRL3_06010	An02g03120	Rab GDI family protein (<i>gdiA</i>)	-	T	C	7 th base of intron 2 (A>G)
IV	NRRL3_06010	An02g03120	Rab GDI family protein (<i>gdiA</i>)	-	A	C	2 nd base of intron 2 (CT>GG)
VII	NRRL3_09701	An11g05430	Hypothetical protein	-	G	A	Codon change: Arg ^{16/365} --> Cys ^{16/365}
VIII	NRRL3_11721	An06g00500	Hypothetical protein	+	CA	TC	Codon change: Gln ^{72/492} --> Ser ^{72/492}

III (*ΔkusA::amdS, JN6.2*) or chromosome VII (*nicB, TLF54*), by scoring all 200 segregants for presence or absence of *nicB*⁺ and *amdS*⁺. Segregation of *nicB*^{+/−} was found to be 102/98, whereas *amdS*^{+/−} segregation was scored to be 84/116 (Supplementary Table 1). These data suggested that the segregation of TLF92 occurred at an approximate 50/50 ratio of chromosomal co-segregation for the genetically marked chromosomes.

3.3 Genome sequencing reveals eight ORF-located SNPs in RD15.8#16

To identify the genotypic relation of the cell wall phenotype of RD15.8#16, we performed genome sequencing of TLF54; the derivative of RD15.8#16 used as mutant parent in the parasexual cross and compared it with the genome sequence of RD15.8. SNP calling was performed as described in section 2.5; a total of 44 SNPs and 9 indels were identified across the genome of TLF54 (Supplementary table 2). Eight SNPs and two insertions were identified to be inside ORFs and nucleotide changes and their respective effect on in protein sequence are listed in Table 2. In addition to coding sequence changes, two genes were found to harbor intron-located mutations.

3.4 Co-segregation analysis of SNPs reveals importance of chromosome IV

Due to the low number of segregants with the mutant phenotype of TLF54, we were unable to perform bulk segregant analysis (BSA) and decided to identify relevant SNPs by performing a SNP co-segregation analysis. Initially, SNPs were determined by sequencing the ORF-located SNPs (Table 2, with the exception of *pyrG*) in mutant segregants *ΔbrnA*#53 and *ΔbrnA*#90, and two segregants that did not display the mutant phenotype (*ΔolvA*#27 and *ΔolvA*#41).

Sequenced SNPs of parental strains and segregants are displayed schematically in Figure 4. Yellow bars represent the SNPs of the wild type, whereas green bars indicate the SNP identified for TLF54. The co-segregation analysis indicated that SNPs associated with chromosome I and IV co-segregate with the mutant phenotype (Figure 4). However, note that the SNP on chromosome I (NRRL3_01084) is located on the same chromosome arm as either color marker *ΔolvA* (wild type SNP) or *ΔbrnA* (mutant SNP), making co-segregation of the *ΔbrnA* color marker, and not the cell wall mutant phenotype, a possible consequence of genetic linkage.

To check whether mutant SNPs on chromosome I (NRRL3_01084) or on chromosome IV (NRRL3_05482 and NRRL3_06010) are co-segregating with the phenotypes, a second set of segregants with wild type-like phenotypes was included for SNP sequencing shown in Figure 4. Only wild type SNPs were found for both NRRL3_05482 and NRRL3_06010 on chromosome IV in segregants that do not display the TLF54 phenotype. These data suggest that the SNPs found on chromosome IV are associated with the phenotypes of RD15.8#16.

3.5 SNPs re-creation shows that the mutant allele of NRRL3_06010/*gdiA* is responsible for the phenotype of RD15.8#16

The SNP co-segregation analysis showed the SNPs on chromosome IV to be associated with either the wild type or mutant phenotype. In addition to NRRL3_05482 and NRRL3_06010, TLF54

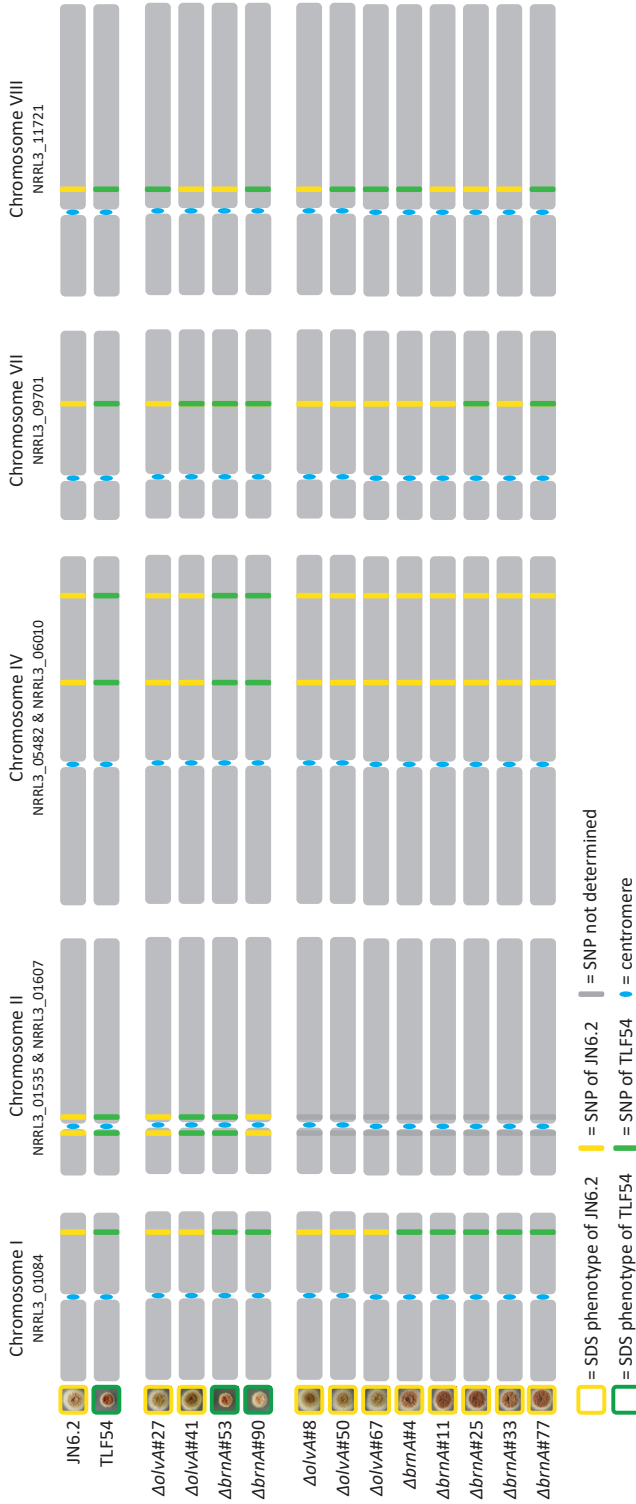


Figure 4. Overview of identified SNPs in JN6.2, TLF54 and 12 segregants based on local sequencing. Parental strains of parasexual cross are listed above; olive colored wild type (JN6.2) and brown colored RD15.8#16 derivative (TLF54). An initial set of four segregants was used to sequence all ORF-related SNPs, previously shown to resemble either the phenotype of RD15.8 #16 or wild type (Figure 3, $\Delta brnA\#53$ and $\Delta brnA\#90$, and $\DeltaolvA\#27$ and $\DeltaolvA\#41$, respectively). A second set of segregants that resemble the wild type phenotype ($\DeltaolvA\#8$, $\DeltaolvA\#50$, $\DeltaolvA\#67$, $\Delta brnA\#4$, $\Delta brnA\#11$, $\Delta brnA\#25$, $\Delta brnA\#33$ and $\Delta brnA\#77$) was sequenced for ORF-related SNPs for chromosome I, IV, VII and VIII. Strains and respective colony morphology are shown on Minimal Medium (MM). Only chromosomes I, II, IV, VII and VIII are shown as they harbor the ORF targeted SNPs (see Table 2). Sizes of chromosomes and SNPs are not to scale, and represent both the approximate length of the chromosomes and the SNP locations. Colored bars are indicative for the inherited SNP; yellow represents the wild type (JN6.2) SNP, whereas the green SNP represents the mutant (TLF54). Gene ID of targeted ORFs are listed below the chromosome number in respective order: Genes NRRL3_06010 (*gdiA*) and NRRL3_11721 both harbor two SNPs within 5bp of one another and are displayed in this figure as a single yellow or green bar (for details see Table 2).

harbors three additional SNPs on chromosome IV (Supplementary table 2), but were all found to be outside of promoter or coding regions. Therefore, we considered the two genes NRRL3_05482 and NRRL3_06010 as candidates for causing the observed cell wall phenotype of RD15.8#16.

Using a split marker approach as described in section 2.7, we attempted to create full gene knockouts. Transformants of both Δ NRRL3_05482::*AOpyrG* and Δ NRRL3_06010::*AOpyrG* in MA169.4 showed low levels of sporulation and single streaking on either selective or non-selective medium often did not show colony forming units derived from single spores, suggesting these genes are essential for growth and the null allele only allows growth through heterokaryotic rescue (Osmani et al., 2006). Transformants that did grow after re-streaking were expected to contain ectopically integrated selection markers, as diagnostic PCR did not show correct deletion of ORF (data not shown).

Based on these results we opted to re-create the mutant SNPs in a wild type background using CRISPR/Cas9 genome editing. This was achieved by targeting either NRRL3_05482 or NRRL3_06010 in the wild type MA234.1 (Table 1) with respective plasmids pFC332_NRRL3_05482-sgRNA and pFC332_NRRL3_06010-sgRNA, and simultaneously present a linear repair DNA fragment from TLF54 that contains the SNPs in question, for homologous recombination.

For NRRL3_06010, we exploited the location of the +2 intronic SNP to create a sgRNA target that targets the wild type SNP, but does not recognize the mutant SNP located on the DNA repair fragment. The +2 intronic G/GT \rightarrow G/GG mutation of the NRRL3_06010 mutant allele is situated at the second nucleotide upstream from the PAM site of the NRRL3_06010-sgRNA target sequence. A schematic representation of this approach for NRRL3_06010 is shown in Supplementary figure 3A and 3B. MA234.1 was transformed with pFC332_NRRL3_06010-sgRNA and a 2142bp linear DNA repair fragment (amplified from genomic DNA of TLF54, with primers OTL485 and OTL486 (Primer Table). Sequencing of the NRRL3_06010 locus in transformants revealed the successful integration of the linear repair DNA fragment (data not shown), yielding strain AG3 with the NRRL3_06010 mutant allele SNPs at the +2 and +7 intronic position (Table 1).

The SNP located in NRRL3_05482 mutant allele did not provide a favorable target site for sgRNA design. Instead, a target that lies 317 bp downstream was used to create plasmid pFC332_NRRL3_05482-sgRNA. To omit recognition of the NRRL3_05482-sgRNA-Cas9 ribonucleoprotein (RNP) complex of the linear DNA repair fragment obtained from NRRL3_05482 mutant allele, we introduced a silent mutation (ACG \rightarrow ACA, Thr) in the target site at the 10th nucleotide upstream from the PAM site (5' – TGG – 3'). This was achieved by *in situ* single mismatch PCR, creating two flanks that were subsequently fused by fusion PCR. A schematic overview of this approach is displayed in Supplementary figure 3C. Using the genomic DNA of TLF54, we used primers to introduce a G to A transition using primers listed in Primer Table. The combined flanks yield a 2499bp linear DNA repair fragment from NRRL3_05482 mutant allele with an additional SNP in Thr⁻³¹⁸ (ACG to ACA: NRRL3_05482^{Thr318(ACA)}) at the target site of NRRL3_05482-sgRNA, and was sequenced to confirm this addition (data not shown). MA234.1 was transformed with pFC332_

NRRL3_05482-sgRNA and repair DNA fragment NRRL3_05482^{Thr318(ACA)}. Transformants were confirmed using sequencing (data not shown), yielding strain AG1.

Equally aged spore stocks of strains RD15.8, RD15.8#16, AG1 and AG3 were harvested, counted and diluted for a SDS sensitivity spot assay. On MM, it is evident that RD15.8 and AG1 show a similar growth phenotype, whereas AG3 displays the same compact colony phenotype as RD15.8#16 (Figure 5). Moreover, AG3, harboring the mutant allele of NRRL3_06010, also shows sensitivity towards SDS as seen for RD15.8#16 across a range of SDS concentrations, whereas AG1 showed wild type like sensitivity. In addition, measured glucosamine content from isolated cell walls were found to be identically increased for both RD15.8#16 and AG3 over RD15.8 (data not shown). Interestingly, NRRL3_06010 encodes a homolog of the previously identified *Aspergillus nidulans gdiA* (AN5895), a Rab GDI dissociation inhibitor (Abenza et al., 2010; MacKenzie et al., 2005).

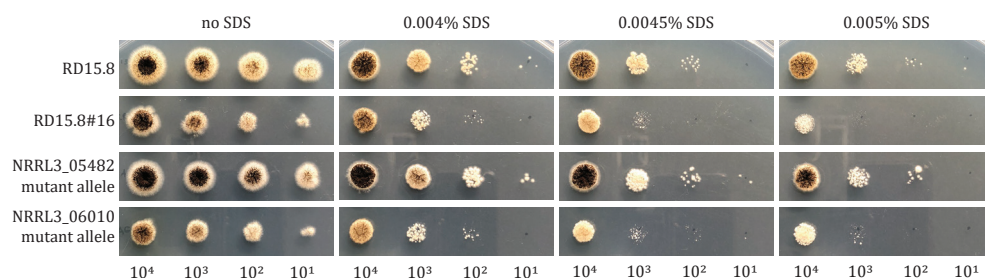


Figure 5. Phenotypes of RD15.8, RD15.8#16, NRRL3_05482 mutant allele (AG1) and NRRL3_06010 mutant allele (AG3). Colony morphology and SDS sensitivity (0.004%, 0.0045% and 0.005%) on Minimal Medium (MM) grown at 30°C for 72h. Spore amounts (#) per spot from left to right are 10^4 , 10^3 , 10^2 or 10^1 , and are listed below the figure. Strains were incubated 96h at 30°C.

3.6 Analysis of *gdiA* mRNA from RD15.8#16 reveals both inefficient and alternative splicing

SNPs in the *gdiA* mutant allele of RD15.8#16 are intronic, showing two SNPs near the 5' donor splice site of intron 2. To assess effects of these mutations on splicing of *gdiA* pre-mRNA (SNPs at the +2 and +7 position, G/GTAGGGA to G/GGAGGGG of the second intron) in RD15.8#16, RNA was isolated from shake flask cultures of both RD15.8 and RD15.8#16 and cDNA was generated using RT-PCR as described in section 2.9. The cDNA of *gdiA* was amplified using PCR (Primer Table) and revealed PCR products for both RD15.8 and RD15.8#16 (data not shown). Next, the purified PCR products were cloned into a pJET1.2/blunt vector. Fourteen clones of RD15.8#16 and of two clones of RD15.8 *gdiA* mRNA (as control) were sequenced using primer 6010_P12r (Primer Table). The two cDNA clones from RD15.8 both carried the fully processed cDNA (https://gb.fungalgenomics.ca/portal/view/geneModelView.php?fullName=NRRL3_06010). Visualization of splicing in wild type and mutant *gdiA* is schematically shown in Figure 6A. For the *gdiA* mutant allele, four different transcripts are observed (Figure 6B). Out of fourteen individual cDNA clones of RD15.8#16, we found that nine carried an un-spliced intron 2, which would result in a premature STOP codon (TGA) located in intron 2, truncating translation of GdiA at 38AA. We also found three instances in which intron 2 was successfully spliced, leading to wild type transcripts. Additionally, two cases of alternative splicing were observed: exon 2 skipping (exon

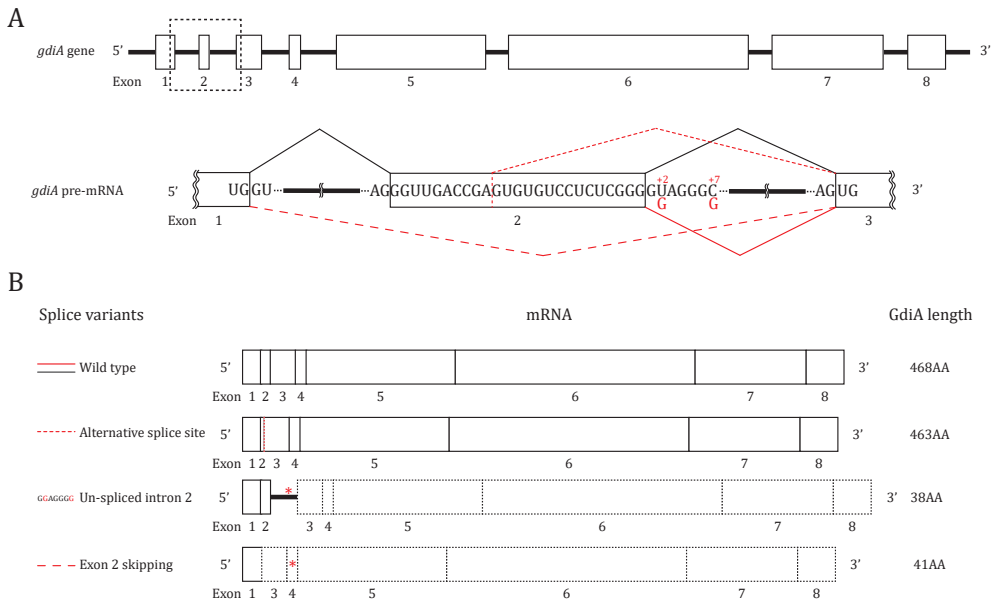


Figure 6. Schematic representation of the *gdiA* gene and the splicing events. (A) The *gdiA* gene consists of 8 exons and 7 introns. Black dashed lines show the region where splicing of *gdiA* pre-mRNA introns 1 and 2 is affected for RD15.8#16 compared to wild type. RD15.8#16 SNPs in *gdiA* of intron 2 at the +2 and +7 position are shown in red. Connecting lines between exons are either shown in black for wild type splicing or red for RD15.8#16 splicing. For RD15.8#16, the solid red line indicates wild type splicing of intron 2, densely interspaced red dashed line represents intron 2 splicing from alternative splice site inside exon 2, and widely interspaced red dashed lines indicate exon 2 skipping. (B) Visualization of resultant mRNA splice variations that have been recorded for both wild type and RD15.8#16 *gdiA* alleles and their corresponding protein length. Red asterisk represents a premature stop-codon. Black dashed line indicates out of frame transcript.

1 joining exon 3) and an alternative splice site in exon 2. Exon 2 (25nt) skipping results in a frameshift that leads to a premature STOP codon (TGA), truncating the protein during translation after 41AA. Interestingly, the alternative splice site found inside exon 2 (GA/GTGTGTCC) results in an in-frame splicing event. This splice variant effectively deletes 5AA (CVLSG) from the 3' end of exon 2, due an alternative splice site upstream from the wild type exon/intron border. Moreover, because of a new exon 2 boundary, the linkage between exon 2 and exon 3 subsequently yields a single nucleotide change that translates in an E19D substitution.

4. DISCUSSION

This work describes the characterization cell wall chitin mutant RD15.8#16 that was obtained from a previously reported cell wall stress mutant library (Damveld et al., 2008). Disturbance of cell wall integrity has been reported to induce cell wall chitin deposition in filamentous fungi (Fortwendel et al., 2010; Heilmann et al., 2013; Ram et al., 2004; Walker et al., 2015, 2008), and was exploited for a screen to identify high chitin producing strains. RD15.8#16 produces 60% more cell wall chitin than wild type *A. niger* and, in addition, displays sensitivity to SDS which is known to disturb the cell wall at low concentrations (De Groot et al., 2001; de Nobel et al.,

2000; Delley and Hall, 1999). These phenotypes, along with a compact colony morphology, were used in a classical genetics approach by employing co-segregation analysis to identify causative mutations.

For co-segregation analysis, a diploid was obtained from a wild type derivative JN6.2 (Δ nicB::A*OpyrG*, Δ olvA::hygB) and mutant TLF54 (a *pyrG*- and Δ *brnA* derivative of RD15.8#16) in a parasexual cross to mix wild type and mutant chromosomes, followed by subsequent segregation. Co-segregation of the mutant phenotype among the acquired segregants was scored using sensitivity to SDS. Prior to this, we confirmed similar SDS sensitivity of both TLF54 and JN6.2 compared to their respective prototrophic counterparts, RD15.8#16 and RD15.8. Initial observations on auxotrophic marker segregation suggested equal co-segregation of chromosomes from wild type and mutant, however, unequal segregation of the RD15.8#16 phenotype was observed, resulting in only 2 SDS sensitive segregants from 200 segregants (Δ *brnA*#53 and Δ *brnA*#90). Low frequency of mutant phenotype segregation could not be explained by benomyl sensitivity for haploid parents, as RD15.8#16 was affected similarly to benomyl as JN6.2 (Supplementary figure 1). Though, certain mutant SNP(s) can be unfavorable during diploid to haploid segregation, either related or unrelated to the SDS sensitivity phenotype. In extension of this observation, we wanted to ensure that there was no disconnect between cell wall chitin and SDS sensitivity for these segregants. This was done by comparing glucosamine content of parental strains JN6.2 and TLF54 with Δ *brnA*#53, Δ *brnA*#90 and two randomly picked non-SDS sensitive segregants Δ olvA#27 and Δ olvA#41 (Figure 3B). Results showed that the plate phenotypes (SDS sensitivity and colony morphology) are linked to increased cell wall glucosamine content. SNP co-segregation analysis revealed inherited SNPs from either wild type or mutant in both SDS sensitive and non-SDS sensitive segregants. We were able to identify that ORF-located SNPs recur randomly across segregants, with the exception of SNPs on chromosome IV (Figure 4), only found in segregants Δ *brnA*#53 and Δ *brnA*#90.

Chromosome IV located mutant SNPs lay within NRRL3_05482 (Yeast *PEP7* ortholog, putative fungal transcription factor) and NRRL3_06010, now identified as *gdiA* (Rab GDP dissociation inhibitor) based on homology with *A. nidulans gdiA* (Abenza et al., 2010). Attempts to create single knockouts of both genes was unsuccessful and suggests them to be essential for growth. In congruence with yeast literature, the ortholog of *gdiA* (*GDI1*) is a known essential gene (Garrett et al., 1994), whereas *PEP7* was previously described as a nonessential gene (Webb et al., 1997). As clean knockout strains could not be obtained, we re-created SNPs found in both NRRL3_05482 and *gdiA* for RD15.8#16 in a wild type background, in order to study their phenotypic effects. Re-creation of SNPs in NRRL3_05482 and *gdiA* through CRISPR/Cas9 gene editing resulted in viable mutants AG1 and AG3, respectively. Interestingly, only AG3 showed the same level of SDS sensitivity as RD15.8#16, suggesting that the SNPs in the *gdiA* mutant allele at the conserved 5' splice site (+2 and +7 position, G/GTAGGGG to G/GGAGGGG) of the second intron, facilitates both the SDS and cell wall chitin phenotype. The data also indicates that the SNP in the NRRL3_05482 mutant allele co-segregated with the *gdiA* mutant allele as a result of chromosome IV linkage, but is not causative for the RD15.8#16 phenotype.

The T to G SNP in the *gdiA* mutant allele causes a mutated 5' donor splice site. The canonical donor-acceptor splice site pair in fungal introns is 5' GU-AG 3' (Kupfer et al., 2004). In addition, non-canonical splice sites are observed sporadically being either 5' GC-AG 3' or 5' AU-AC 3', the former of which represents approximately 90% of non-canonical type splice sites (Bursset et al., 2000). This non-canonical splice site was reported to represent 1.2% of all introns in *Neurospora crassa* with similar ratios for filamentous fungi *Fusarium oxysporum* and *Aspergillus nidulans* (Rep et al., 2006). The 5' GG-AG 3' type splice sites in intron 2 of the *gdiA* mutant allele is different from either of these canonical or non-canonical splice sites. Specifically, a G at second position of the 5' donor splice site (G/GG) has previously been shown to result in failure of proper lariat formation for correct transcript processing (Aebi et al., 1987). However, here we show that the 5' donor splice site in the *gdiA* mutant allele can result in correct pre-mRNA processing. However, failure of intron 2 splice site recognition was more frequently observed. Interestingly, we also found two cases of alternative splicing: exon skipping and an alternative splice site. The latter variant results in a full-length protein that combines a five amino acids deletion with a single amino acid substitution of glutamic acid to aspartic acid. For now, it remains unknown whether this mRNA yields a functional protein and whether other splice variants may exist. Nevertheless, we have found wild type mRNA transcripts for *gdiA*—that are derivative of the mutant allele, suggesting that RD15.8#16 still produces intact, albeit less GdiA. These findings comply with the fact that total loss of *gdiA* mRNA is lethal.

Rab *gdiA* encodes a GDP-dissociation inhibitor that functions as a regulator in Rab GTPase cycling. Known orthologs are conserved and have been reported as essential genes in both yeast and *Drosophila* (Garrett et al., 1994; Ricard et al., 2001). Rab (*rags* from rat brain (Touchot et al., 1987)) GTPases are involved in regulation of intracellular vesicular transport, continuously cycling between and active GTP-bound, and inactive GDP-bound form (Pfeffer, 1992). In the active GTP-bound form, a GTPase is able to interact with downstream effector proteins, assist in cargo selection, transport vesicles, form vesicles from membranes and assist fusion of vesicles with the target membranes (Oesterlin et al., 2014). Once an active GTPase has performed a downstream trafficking cycle at a specific target site, it is subsequently hydrolyzed to a GDP-form. Here, Rab GDIs can solubilize GDP-bound GTPases from membranes into the cytosol prior to re-deposition at new target membranes. Solubilization by GDIs also prevents turnover of GDP to GTP by GEFs, helping to keep an intracellular steady-state balance of active/inactive GTPases (Pfeffer and Aivazian, 2004; Ullrich et al., 1993). Due to the essential role of GdiA in this balancing act, we propose that a reduction in available GdiA—resultant from inefficient pre-mRNA processing—causes a cytosolic imbalance of soluble GTPases.

Obviously, the essential role that GDP dissociation inhibitors have in cellular processes make them difficult to study their function. In *A. niger*, *gdiA* was reported to be repressed by the during exposure of dithiothreitol (DTT), known to disturb cellular redox homeostasis and trigger the unfolded protein response (MacKenzie et al., 2005). In yeast, a conditional mutant *sec19-1* (allelic to *GDI1*) has been studied and has helped to understand its biological function (Garrett

et al., 1994). Resultant phenotypes include accumulation of ER, Golgi and secretory vesicles as well as defects in protein transport and loss of soluble Rab GTPase Sec4p. Although no cell wall phenotypes have been described for the *sec19-1* mutant directly, a conditional mutant of *SEC4* (*sec4-8*), showed random budding patterning, suggesting loss of secretion polarity, an enlarged bud neck and displayed abnormal chitin deposition (Finger and Novick, 1997). Sec4p is an essential protein required for vesicle-mediated exocytic secretion and autophagy (Guo et al., 1999), and relies on the ability to continuously cycle between GTP and GDP, rather than absolute levels of GTP-bound form for proper function (Novick et al., 1993). Unsuccessful release of GDP-bound Sec4p from target membranes as a result of loss or depletion of *GDI1* depletes the soluble pool required for re-activation and re-positioning on new target membranes, rendering Sec4p dysfunctional. Consequentially, putative GDP to GTP exchange of old, *in situ* membrane-bound Sec4p may misallocate protein trafficking, including putative cell wall chitin biosynthesis enzymes. Despite Sec4p and *GDI1* involvement in vesicle trafficking, to the best of our knowledge no reports have investigated its role in cell wall biosynthesis or the cell wall integrity pathway.

In *A. niger*, the closest homolog of Sec4p is secretion related GTPase A (*srgA*, 58% protein identity) and, unlike in yeast, was found to be a non-essential gene (Punt et al., 2001). The *srgA* gene was unable to complement a *sec4* mutant, suggesting the presence of an additional *SEC4* homolog or that *SEC4* in yeast governs more vesicle sorting processes than in *A. niger*. Overall *srgA* may be related to a more complex multicellular growth behavior (Punt et al., 2001). Interestingly, a deletion of *srgA* resulted in changes of colonial and peripheral hyphae morphology, similar to RD15.8#16. The compact colony morphology caused by the mutant allele of *gdiA* in RD15.8#16 may be indirectly related to a regulatory imbalance caused by less GdiA, possibly affecting *SrgA* cycling. Whether or not there is a relation between *srgA* and *gdiA*, we observe an effect of the *gdiA* mutant allele on cell wall chitin deposition. The fact that *A. niger* only contains a single genomic copy of a Rab GDI we conclude that less available GdiA as observed in RD15.8#16 affects the Rab GTPase-mediated vesicle trafficking. Consequently, disturbance of these regulatory elements in Rab GTPase cycling most likely causes multiple pleiotropic effects, among which is cell wall chitin biosynthesis.

5. CONCLUSIONS

RD15.8#16 was initially isolated in a screen for strains with a continuous state of cell wall stress and, upon further analysis, was found to have increased chitin levels and an increased sensitivity to SDS. Using classical genetics combined with co-segregation analysis and CRISPR/Cas9 gene editing, we showed the involvement of two intronic mutations in *gdiA* that give rise to this phenotype. It was found that a full gene disruption of *gdiA* was lethal, and that the observed mutations in the *gdiA* mutant allele affect intron splicing resulting in reduced levels of functional *gdiA* transcript. Therefore, we propose that reduced levels of GdiA affect the balance of Rab GTPase cycling. As such, this either influences cell wall chitin deposition directly through increased

(ectopic) secretion or indirectly, by general misconstruction (and recycling) of fungal cell wall components that triggers the CWI pathway with a compensatory chitin deposition response. Both hypotheses are not mutually exclusive, but are in congruence with an asymmetrical distribution in GTPase cycling. To address the issue in more detail, the reported *gdiA* mutant allele may provide a valuable candidate to study the role of GdiA in secretion-related processes of *A. niger* and other filamentous fungi.

Acknowledgements

We would like to thank Prof. Dr. Bruno M. Moerschbacher for the coordination of the FunChi project.

Funding

This work is part of the “FunChi” ERA-IB project with project number ERA-IB-15-080, which is (partly) financed by the Dutch Research Council (NWO).

Availability of data and materials

The DNA reads described in this study will be deposited in the short read archive upon request. All other data are available on request by contacting the corresponding author.

SUPPLEMENTARY TABLES

Supplementary tables to this article can be found online at <https://doi.org/10.1016/j.fgb.2019.103319>

Primer Table. All primers used during this study.

Supplementary table 1. All $\Delta olvA\#$ and $\Delta brnA\#$ segregants scored for *pyrG*^{+/−}, *nicB*^{+/−} and *amdS*^{+/−} selection marker inheritance.

Supplementary table 2. All 53 SNPs found for TLF54 (VARIANT 004, Mutant) compared to RD15.8 (VARIANT 003, Parent). Frequency cut-off of mutant was performed as described in section 2.5.

SUPPLEMENTARY DOCUMENTS

Supplementary document 1. Detailed protocol for cell wall isolation and total glucosamine determination.

Cell wall hydrolysis and chitin analysis

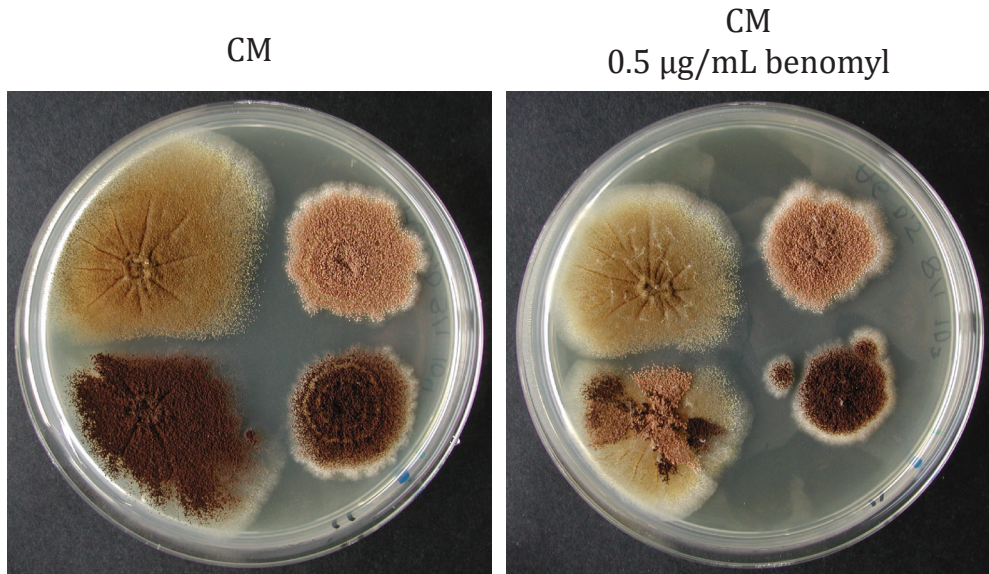
Cell walls of fungal strains were carefully weighed on a fine balance ($d = \pm 0.1$ mg) to be exactly 1.0 mg in a 2 mL Eppendorf tube. Tubes were supplied with a lid cap to secure a closed lid, and were wrapped with PARAFILM® M (Sigma Aldrich). Hydrolysis was performed in triplicate per biological replicate with 1 mL 6M HCl for 4h at 110°C, using a pressure cooker. After cooling down, PARAFILM® M and lid caps were removed and HCl was evaporated at RT for 64h, using an airstream with a Sample Concentrator (Techne Ltd, Cambridge, UK) in the fume hood. To

measure total glucosamine in samples, a Glucosamine HCl standard was included, performed in triplicate*: using a 10 mg/mL stock dilutions of 2000 µg/ml, 1500 µg/ml, 1000 µg/ml, 500 µg/ml, 250 µg/ml, 100 µg/ml, 50 µg/ml and 0 µg/ml (in triplicates) were made. Dried, hydrolyzed cell walls were rehydrated in 500 µL MQ (2 mg/mL cell wall) and incubated for 1h at 37°C, 1,000 rpm, simultaneously with standards. Post-incubation, 20 µL sample (40 µg cell wall hydrolysate) and freshly prepared standards (40, 30, 20, 10, 5, 2, 1 and 0 µg glucosamine) were taken in triplicate and added to freshly prepared 20 µL 1.5N Na₂CO₃ in 4% acetylacetone** in PCR tubes (250 µL), followed by 20 min. incubation at 100°C. Next, 140 µL 96% EtOH was added to cooled down samples and standards. In the fume hood, 20 µL 4-dimethylaminobenzoaldehyde solution (0.64g 4-dimethylaminobenzoaldehyde in 12 ml 96% EtOH and 12 ml concentrated HCl**) was added to samples and standards which colors the solution pink. To allow the reaction to reach optimal coloring intensity, samples and standards were incubated 1h prior to transferring 100 µL solution to a 96-well plate, and OD520 was measured in a plate reader. Standard curve samples range from OD520 = 0 (set intercept) to OD520 = 1 for the highest concentration (2000 µg/mL, i.e. 40 µg glucosamine). Plotting a linear standard curve, total glucosamine content in each sample was inferred.

*NOTE: 6M HCl hydrolysis liberates chitin from the cell wall, but also removes acetyl groups. Essentially, this protocol looks at total glucosamine instead of just free N-acetylglucosamine monomers (no differentiation between chitin and chitosan). Glucosamine monomers can be reactive with surfaces and undergo reactions with other chemicals that may skew the colorimetric read-out. Therefore, it is important to create fresh stocks of glucosamine standards, and that both standards and dissolved cell walls are incubated for an equal amount of time under the same conditions.

** NOTE: It is of very high importance to create fresh solutions every single time this experiment if performed for the sake of reproducibility. Na₂CO₃ (1.5N) in 4% acetylacetone tends to discolor quickly over the course of a couple of days and alters the outcome of the read-out. The degrading effect of 4-dimethylaminobenzoaldehyde in concentrated HCl and EtOH is not completely clear. However, to avoid variation between experiments creating fresh, small volumes of both solutions every single time ensures good reproducibility. This is based on personal experience and that was reflected in standard curves.

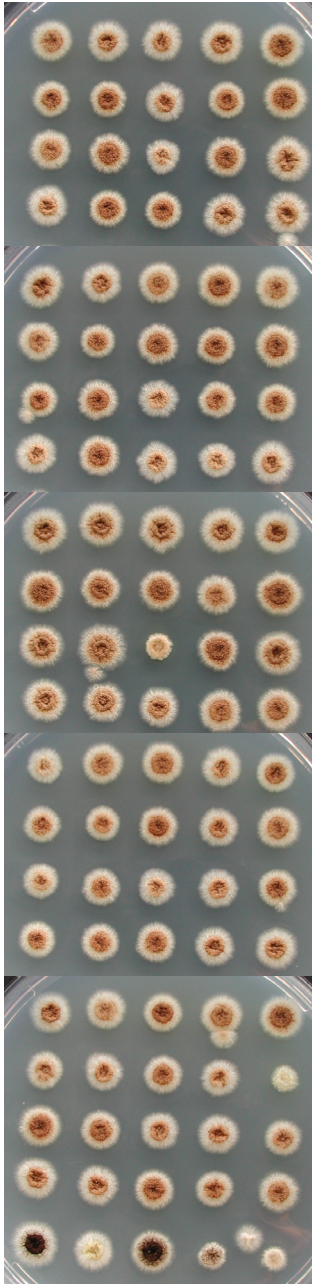
SUPPLEMENTARY FIGURES



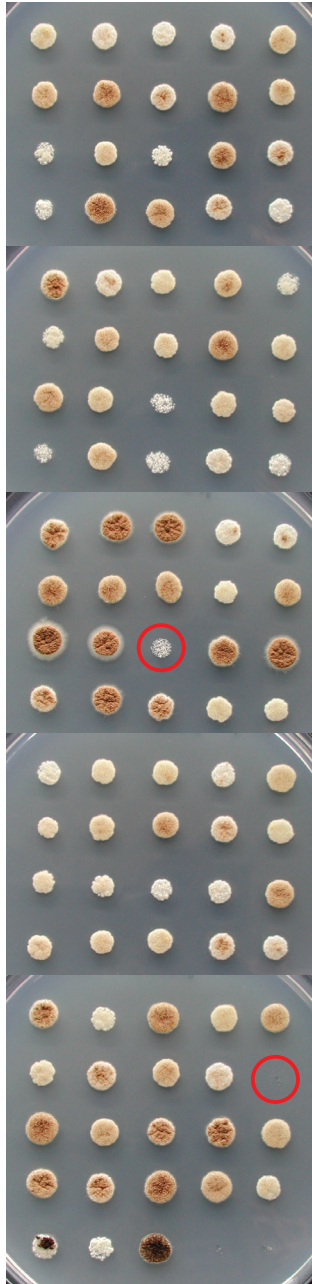
Supplementary figure 1. Growth on CM and CM with benomyl. From left to right, top to bottom: JN6.2, TLF54, TLF92 diploid and RD15.8#16 on CM and 0.5 µg/mL benomyl. Note segregation of diploid phenotype into brown and olive colored sectors.

A

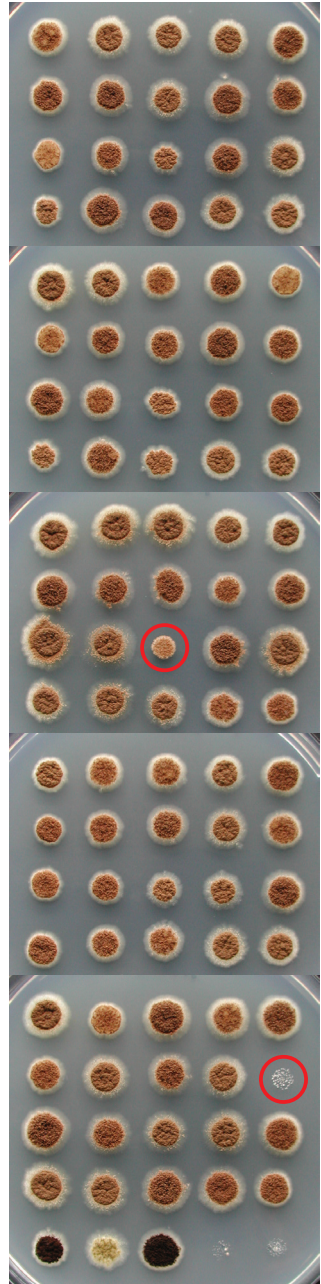
72h
MM + U + N

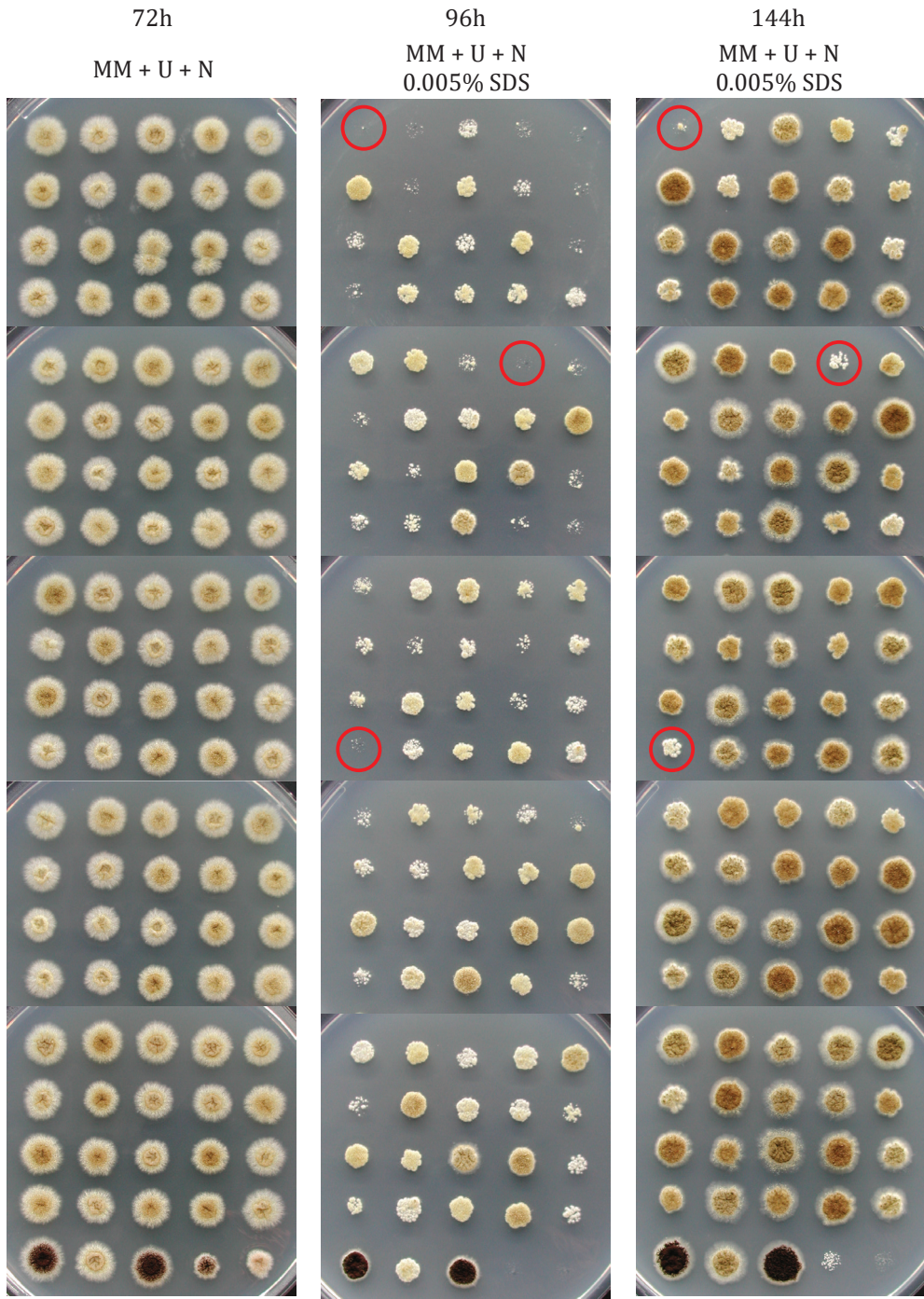


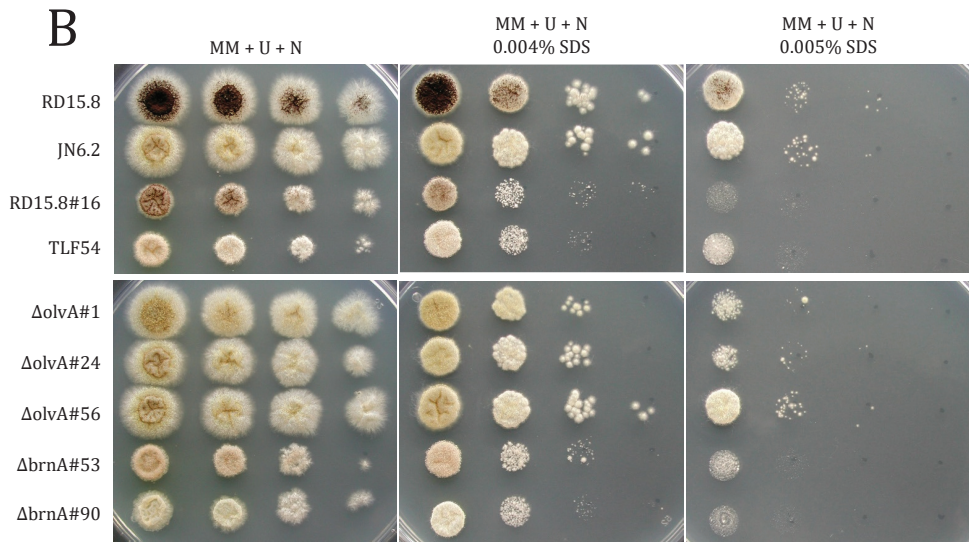
96h
MM + U + N
0.005% SDS



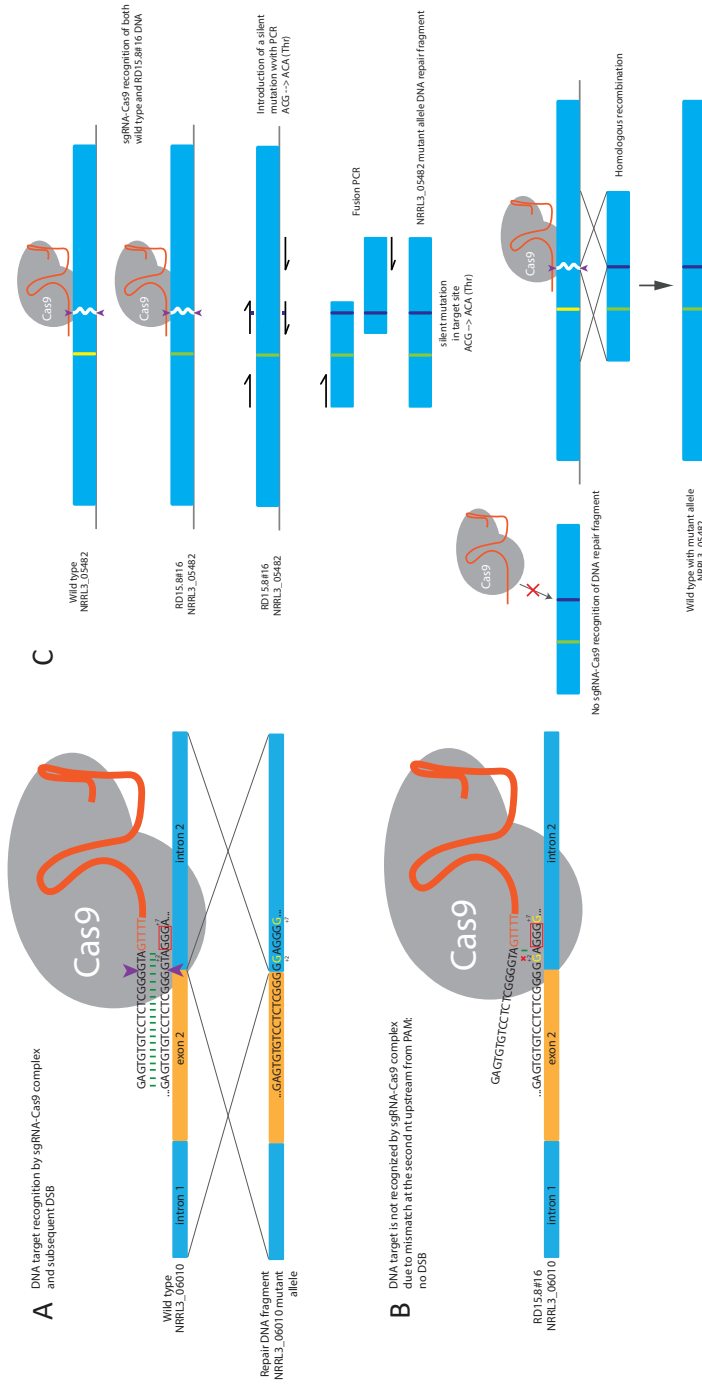
144h
MM + U + N
0.005% SDS







Supplementary figure 2. Screen of 200 segregants and control strains with un-normalized spore concentrations. All plates contain Minimal Medium (MM) with 10mM uridine (U) and 2.5 μ g/mL nicotinamide (N) + 0.005% SDS. (A) A total of 200 segregants and controls were spotted (5 μ L) with controls at the bottom (from left to right on bottom of each plate: N402, JN6.2, RD15.8, RD15.8#16 and TLF54). Segregant IDs are brnA#1-100, followed by olvA#1-100 from left to right, top to bottom. Red encircled spore spots resemble putative candidates that exhibit SDS sensitivity. (B) Putative SDS sensitive candidates on a normalized spore SDS spot assay. Plates were incubated for 72h at 30°C.



Supplementary figure 3. CRISPR/Cas9 design for targeting of NRRL3_06010 and NRRL3_05482 to re-create SNPs in a wild type background. (A) NRRL3_NRL3_06010-sgRNA-Cas9 ribonucleoprotein (RNP) complex binds the genomic DNA of the wild type strain, creating a DSB in *gdiA*. PAM site is highlighted by a red box (GGG). Green bars represent matching of bp between the sgRNA target and genomic sequence. Purple arrows indicate the site of the double stranded break (DSB). Repair DNA fragment contains the two point mutations found in RD15.8#16 and are shown in yellow. (B) The mutant allele NRRL3_06010 sequence from RD15.8#16 shows a mismatch at the second nucleotide (nt) upstream from the PAM site, displayed by a red cross; preventing the NRRL3_06010-sgRNA-Cas9 RNP complex to bind and create a DSB. (C) NRRL3_05482-sgRNA-Cas9 RNP complex targets a region outside of the NRRL3_05482 SNP location. SNPs are shown as either yellow (wild type) or green (RD15.8#16). To prevent recognition and cutting of the DNA repair fragment a silent mutation (ACG → ACA (Thr)) is introduced at the target site of NRRL3_05482-sgRNA, with fusion PCR. The NRRL3_05482-sgRNA RNP complex creates an in vivo DSB at the wild type locus, but not at the presented DNA repair fragment, allowing repair of the DSB through homologous recombination.

